Direct observations of wave-sea ice interactions in the Antarctic Marginal Ice Zone

S. Wahlgren[1], J. Thomson[2], L. C. Biddle[1,3], S. Swart[1]

[1]Department of Marine Sciences, University of Gothenburg, Gothenburg, Sweden
[2]Applied Physics Laboratory, University of Washington, Seattle, Washington
[3]Voice of the Ocean, Gothenburg, Sweden

Key Points:

- SWIFT buoy data show that frequency dependence of wave attenuation in sea ice follows a power law, with exponent 3-4.
- Both wave attenuation and the frequency dependence of attenuation were stronger in winter than in spring.
- Observations suggest a change in wave direction as a function of distance from the sea ice edge.

Corresponding author: Stina Wahlgren, `stina.wahlgren@gu.se`

Abstract

Wave energy propagating into the Antarctic marginal ice zone affects the quality and extent of the sea ice, and wave propagation is therefore an important factor for understanding and predicting changes in sea ice cover. Sea ice is notoriously hard to model and in-situ observations of wave activity in the Antarctic marginal ice zone are scarce, due to the extreme conditions of the region. Here, we provide new in-situ data from two drifting Surface Wave Instrument Float with Tracking (SWIFT) buoys deployed in the Weddell Sea in the austral winter and spring in 2019. The buoy location ranges from open water to more than 200 km into the sea ice. We estimate the attenuation of swell with wave periods 8-18 s, and find an attenuation coefficient $\alpha = 4 \cdot 10^{-6}$ to $7 \cdot 10^{-5}\,\mathrm{m}^{-1}$ in spring, and approximately five-fold larger in winter. The attenuation coefficients show a power law frequency dependence, with power coefficient 3.3 in spring and 4 in winter. The in-situ data also shows a change in wave direction, where wave direction tends to be more perpendicular to the ice edge farther into the sea ice. A possible explanation for this might be a change in the dispersion relation caused by changing sea ice composition. These observations can help shed further light on the influence of sea ice on waves propagating into the Marginal Ice Zone, aiding development of coupled wave-sea ice models.

Plain Language Summary

Changes in the sea ice extent around Antarctica affects the global climate, and it is therefore important to accurately represent sea ice in climate models. One feature that is generally missing in climate models is the interaction between ocean waves and sea ice. Ocean waves change the sea ice, for example by breaking up ice floes into smaller ones. At the same time, the sea ice reduces the strength of the waves so that the wave height decreases and eventually disappears far into the sea ice. How far into the sea ice waves reach depends both on the size of the waves and on the sea ice. Due to the complexity of sea ice, theoretical models of how waves and sea ice interact are still in development. In order to better represent the wave-sea ice interactions in climate models, simple but accurate models of how fast sea ice reduces the strength of waves is needed. Using two wave buoys, we measured the wave activity in the Antarctic sea ice during two expeditions in 2019. Together with similar measurements from other parts of the Antarctic sea ice, this can help to improve predictions of sea ice cover.

1 Introduction

The sea ice around Antarctica is important for global climate in several ways. Loss of Antarctic sea ice has been linked to ice shelf disintegration, by allowing storm-induced swell waves to reach exposed ice shelf fronts, leading to accelerating loss of the Antarctic ice sheet and increase in sea level rise (Massom et al., 2018). The growth and melt of sea ice acts as a freshwater sink/source, and ocean-atmosphere interactions, such as exchange of heat or momentum, are also affected by the ice condition (Vichi et al., 2019). The transition between the open ocean and permanent sea ice is called the Marginal Ice Zone (MIZ). Multiple definitions of the MIZ exist, depending on purpose and field of study it can be defined based on wave activity as a region where waves and sea ice co-exist (Montiel et al., 2022), based on seasonal ice growth and melt or simply as the region between 15% and 80% sea ice concentration. In the Antarctic the width of this zone can be hundreds of kilometres (Toffoli et al., 2015).

One factor that influences the MIZ and its sea ice condition is surface gravity waves. Waves affect ice formation (Shen & Ackley, 1991/ed) and can break big ice floes into smaller ones (Langhorne et al., 1998/ed), altering dynamical properties and heat exchange. One key property determining to what extent this happens is the significant wave height (Toffoli et al., 2015). In return, the MIZ also affects surface waves by attenuating them, thus influencing how far into the ice the waves reach and can affect the sea ice. Incorporating coupled sea ice-wave models into climate models is therefore important for improving predictions of for example MIZ extent and distribution. Yet, wave-ice coupling is still generally neglected in polar climate modelling (Kousal et al., 2022). Lack of observations also leaves weak constraints on models (Cooper et al., 2022), meaning that future predictions and current parameterizations have large uncertainties.

It is well established that the amplitude of waves decreases with distance travelled in ice, and that the sea ice acts as a low-pass filter, attenuating higher frequency waves more rapidly than waves with lower frequencies. The exact nature of the attenuation, and how much of it that can be attributed to energy dissipation versus scattering, has long been debated (Squire, 2018)(Thomson, 2022), but recent observations point to dissipation as an important factor (Ardhuin et al., 2020)(Voermans et al., 2019). Waves travelling into the MIZ are typically thought to decay exponentially, which was first reported in (Wadhams et al., 1988) based on several field experiments in the Arctic MIZ. Since then, many studies have reproduced this result. There are some observations of linear decay for long wavelengths and high significant wave height (Montiel et al., 2018)(Meylan et al., 2014), which might reflect non-linear phenomena or be artefacts due to small data sets and different ice conditions (Kohout et al., 2020). Many studies have shown a so-called "roll over" effect, where attenuation is not decreasing with increasing frequency for all frequencies. This roll-over effect has recently been explained in (Thomson et al., 2021) as an artefact due to frequency dependent modulation noise, introduced in data collection and signal processing. Wind-generated waves in sea ice could also have contributed to the observed roll-over effect (Li et al., 2017).

The frequency dependence of the attenuation is typically modelled as a power law dependence, or as a sum of power laws. Different physical processes are expected to result in different frequency dependence. Observations from both the Arctic and the Antarctic MIZ consistently shows a power coefficient between 2 and 4 (Meylan et al., 2018), affected by physical parameters such as sea ice type and concentration, floe size and wave period (Montiel et al., 2022) (Kohout et al., 2020)(Meylan et al., 2018). W. E. Rogers et al. (2021), found a strong positive correlation between attenuation and sea ice thickness. Further, Ardhuin et al. (2020) emphasise that attenuation mechanisms differ vastly between the outer break-up region, where waves cause the sea ice to form floes, and the inner region with continuous ice sheets. Wind direction can also influence attenuation, where head-wind has been observed to increase attenuation (Montiel et al., 2022).

Observations of frequency dependence attenuation in the Antarctic MIZ are scarce. Meylan et al. (2014) described the attenuation coefficient for wave periods 2-20 s as a sum of two power laws of order 2 and 4, based on data from an array of 5 wave buoys deployed in September 2012 during the SIPEX-II campaign. The most extensive wave buoy data set is from the PIPERS expedition, where 14 buoys were deployed in the Ross Sea, collecting data between April and July 2017 (Kohout et al., 2020). Neither of these wave buoys provide wave direction. W. E. Rogers et al. (2021) used a subset of the PIPERS data set, collected in June 2017. Montiel et al. (2022) found a power coefficient 2.5 based on another subset of the PIPERS data set collected in April-May 2017.

In this study we present new wave buoy data from the Weddell Sea. We use this to derive frequency dependent attenuation in the Antarctic MIZ for both austral winter and spring. We also show a correlation between wave direction and distance to the ice edge that might be attributed to a change in the dispersion relation.

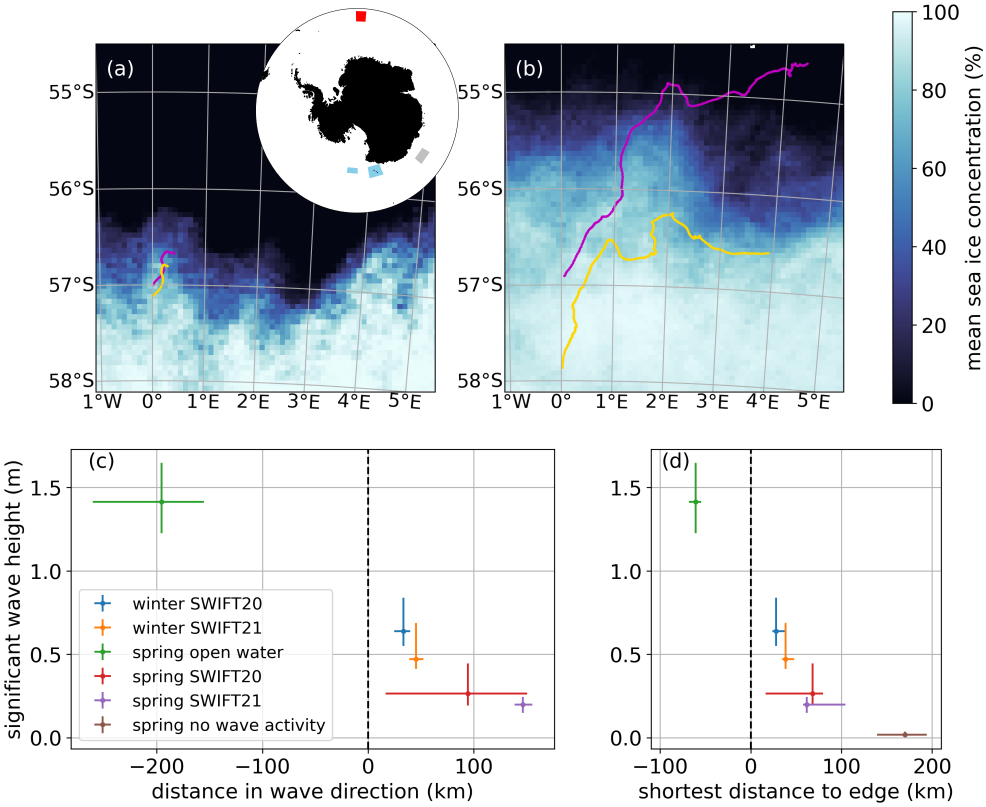

Figure 1. Overview of the two SWIFT deployments. Average sea ice concentration over the time span the buoys were deployed, together with tracks for SWIFT20 (magenta) and SWIFT21 (yellow), during a) winter deployment and b) spring deployment. Inset: Geographic location of the SWIFT deployments (red), together with the locations of the PIPERS data set (light blue) (Kohout et al., 2020) and SIPEX II data set (grey) (Meylan et al., 2014). c) Median and quartiles of significant wave height for all four deployments as a function of distance to ice edge in the energy-weighted wave direction, as measured by the buoy. The SWIFT20 spring deployment is split into in-ice (SIC $\geq$ 15%) and open water (SIC $<$ 15%). d) Same as c, but as a function of the shortest distance to the ice edge. Data with no measurable wave activity ($H_s < 0.1$m) is shown in a separate category.

2 Materials and Methods

2.1 SWIFT Buoy and Deployments

We use data from two SWIFT v3 buoys (Thomson, 2012) deployed in the MIZ in the Southern Ocean as part of the ROAM-MIZ project (`www.roammiz.com`) during the SCALE research voyages in 2019. The buoys were equipped with GPS logger, inertial measurement units (IMU), meteorological stations (airmar WX-200 Ultrasonic weather stations) and a low resolution camera. The two buoys, here referred to as SWIFT20 and SWIFT21, were deployed in austral winter (July 27-28) and austral spring (October 23 – November 7). They recorded a total of 17 days of data (16 days simultaneously with both buoys) with different ice types and weather conditions. SWIFT buoys are deployed directly into the water, and measure wave periods in the range 2-20 s, corresponding to wavelengths 6-600 m in deep open water. This covers all but the highest frequencies of the wind-wave interactions.

In winter, SWIFT20 was deployed at 57°S, 0°E, approximately 25 km into the sea ice pack. SWIFT21 was deployed approximately 10 km south of SWIFT20, further into the sea ice field, and they stayed approximately 10 km apart while drifting north (Figure 1a). The sea ice consisted of 1-5 m pancakes, around 40 cm thick, with WMO (code 3739) ice age ID3 (predominantly new and/or young ice with some first-year ice) (Skatulla et al., 2022). Photos of the ice taken from the ship are provided by (de Vos et al., 2019). The edge of the MIZ was further south in the winter than during the spring deployment, and was advancing north during and after the winter deployment.

For the two week long spring deployment, SWIFT20 was deployed at the same site as the winter deployment, which was then around 100 km from the ice edge. The sea ice consisted of 1-5 m ice floes with slush in between. SWIFT21 was deployed around 100 km south of SWIFT20 (Figure 1b), in the ship track in densely packed, consolidated ice floes. Again, both buoys drifted north. After approximately 9 days, SWIFT20 drifted out of the ice into open water, while SWIFT21 stayed in the sea ice during the deployment. On recovery of SWIFT21, the sea ice consisted of 1-5 m ice floes with water present between the ice floes. Photos from deployment and recovery are presented in the supplementary material (Figure S1-S3).

2.2 Wave spectrum

SWIFT buoys estimate the wave field by measuring the horizontal (GPS) and vertical (IMU) displacement of the buoy. The power spectral density, $E(f)$, is derived from the displacements by assuming a circular orbital motion (Thomson et al., 2018), which is predicted by linear wave theory for waves in deep open water. The validity of this assumption is measured with the check factor, which is simply the ratio between the measured horizontal and vertical displacement (Thomson et al., 2015). This ratio should be equal to 1, and large deviations from this indicates that the measurement is not reliable.

Significant wave height, H_s, is computed from the wave spectrum with

$$H_s = 4 \cdot \sqrt{\int E(f)\,df}, \tag{1}$$

Data with $H_s < 0.1\,\mathrm{m}$ is not used in further analysis due to low signal-to-noise ratio (SNR).

In addition to the 1D wave spectrum, SWIFT buoys provide the standard directional moments of the spectrum (a_1, b_1, a_2, b_2). The dominant direction for each frequency bin can be derived from the cross correlation of the displacements (both horizontal and vertical) using the first directional moments a_1 and b_1 (see the appendix in Thomson et al. (2018) for details). We define the mean wave direction, Θ, for a frequency band limited by f_1, f_2 as the energy weighted dominant direction

$$\Theta = \arctan\left(\bar{b}_1, \bar{a}_1\right), \tag{2}$$

where

$$\bar{a}_1 = \frac{\int_{f_1}^{f_2} E(f) a_1(f)\, \mathrm{d}f}{\int_{f_1}^{f_2} E(f)\, \mathrm{d}f} \tag{3}$$

is the energy weighted directional moment. The spread of the mean direction, $\Delta\Theta$, is computed as

$$\Delta\Theta = \sqrt{2\left(1 - \sqrt{\bar{a}_1^2 + \bar{b}_1^2}\right)}. \tag{4}$$

2.3 Defining the ice edge

In order to determine the distance travelled by waves in sea ice, we need to estimate the location of the transition between open water and the MIZ, here called the sea ice edge. We estimate the ice edge based on AMSR-E sea ice concentration (SIC). The dataset had a spatial resolution of 6.25 x 6.25 km and provided daily (Melsheimer & Spreen, 2019). The sea ice concentration was interpolated to hourly resolution in order to match the SWIFT data. The AMSR-E sea ice concentration was compared to SAR images (GRD, HH-band) from Sentinel-1 (0.1 x 0.1 km, 6 day resolution) when available in our study region. Sea ice concentration and SAR images showed good agreement compared to the sea ice extent (Figure 2a).

The ice edge was detected from sea ice concentration as follows: for each time instance, a binary map was created, with zeros where sea ice concentration was less than 15 % and ones where sea ice concentration was 15 % or more. The binary map was then smoothed using a 2D Gaussian filter with a standard deviation σ_{edge} of 1 pixel (6.25 km), and the ice edge was defined as the 0.5 contour line of the smoothed map. An example of sea ice concentration and derived ice edge is shown in Figure 2b.

The ice edge was roughly aligned in the east-west direction, but was observed to be very dynamic in its orientation and location. During the spring deployment, the ice edge shifted more than 100 km north during the first 6 days, illustrating that the Antarctic MIZ is prone to large spatial changes over short periods (Figure 2c).

2.4 Local ice condition

In addition to co-located AMSR-E sea ice concentration data, imagery from cameras mounted on the masts of the SWIFT buoys were used to categorise the local ice condition (Figure 3). The cameras were approximately 1 m above the surface, and captured one photo every 4 seconds for the first 8 minutes of every hour. The images were analysed manually. Photos captured during the dark hours (around 8pm - 4am local time for the Spring deployment), as well as blurry photos were discarded. The blurriness often occurred during morning hours and typically disappeared after a couple of hours, probably due to ice on the lens. Time lapses of the imagery are provided in the supplementary materials (Movie S1-S3).

Due to limitations of the imagery, existing established ice scales, such as the Antarctic Sea Ice Processes and Climate (ASPeCT) protocol were not applicable. The main limitations are a limited field of view and no available size reference (except for a few feathery friends - Figure 3), which makes it hard to determine ice thickness and floe size. An ice type scale designed specifically for SWIFT imagery was introduced in W. Rogers et al. (2018) (Hošeková et al., 2020), but this only covers pancake ice. We therefore developed a new ice scale (Table 1). The scale is inspired by the ASPeCT protocol and uses

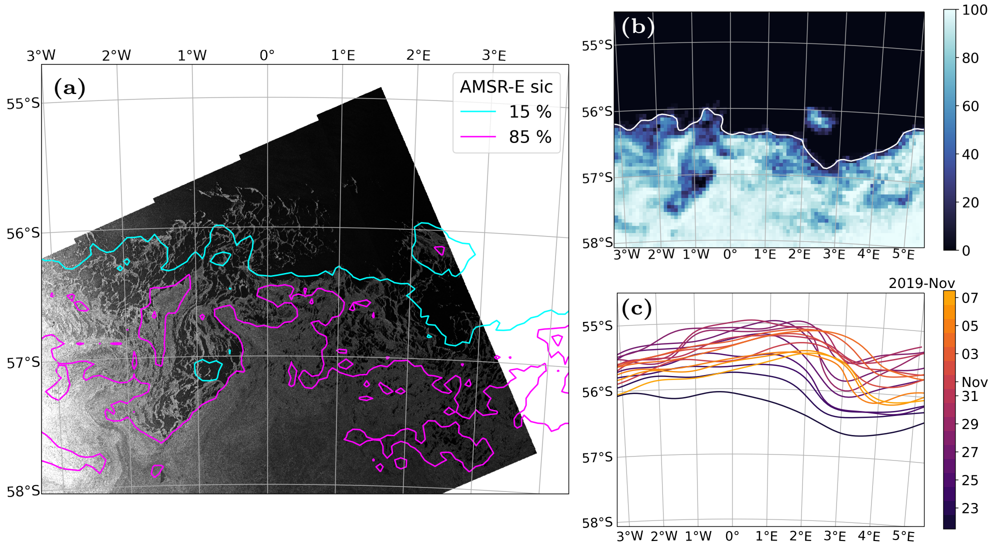

Figure 2. Locating the ice edge from AMSR-E sea ice concentration. a) Comparison between sea ice concentration and Sentinel-1 SAR imagery. b) Example of ice edge (white) derived from AMSR-E sea ice concentration. c) The movement of the ice edge during the spring deployment. For illustration purposes, a smoother version of the edge ($\sigma_{\text{edge}} = 37.5\,\text{km}$) is shown.

Table 1. Ice scale used for quantifying local ice condition based on SWIFT buoy on-board imagery.

Ice Code	Description
-1	Open water patch deep in sea ice
1	Open water
2	Open water and trace ice
3	Small pancakes (<1m)
4	Brash
5	Ice cakes/floes with frazil or open water
6	Ice cakes/floes with brash
7	Tightly packed ice cakes/floes

terminology as defined in World Meteorological Organisation (WMO) Sea-Ice Nomenclature. Example imagery is shown in Figure 3. Based on the imagery, each hour was assigned an ice code (Figure 4).

2.5 Distance to the edge

The peak wave direction measured with SWIFT was generally towards south east, indicating an oblique incidence from the ice edge. We use two different measures of distance to the ice edge: the shortest distance to the edge and the distance in respect to the wave direction. The latter one is the one that matters for wave attenuation, but it is also sensitive to errors in estimated wave direction. For determining wave direction, the energy-weighted mean wave direction was used, as defined in equation 2 at the buoy

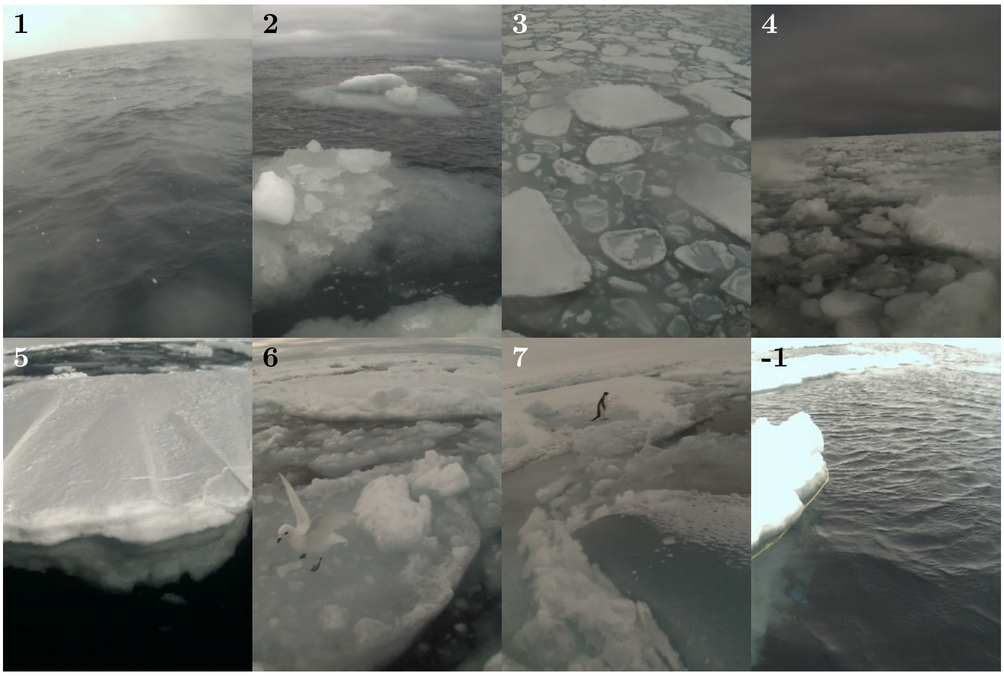

Figure 3. Examples of SWIFT on-board imagery and ice codes.

location. Distance in wave direction was not computed for data points with $H_s < 0.1\,\text{m}$, since no reliable wave direction could be derived for those points.

Distance was determined in AMSR sea ice concentration coordinates. This is a polar stereographic projection, referenced at 70°S, 0° (Melsheimer, 2019), thus giving a distortion of 11-12% at the buoy location. Compared to other uncertainties, this is small and therefore not accounted for.

2.6 Wave attenuation

We derive spectral wave attenuation assuming exponential decay with distance:

$$E(d, f) = E_0(f)e^{-\alpha(f)d}, \tag{5}$$

where $\alpha(f)$ is the (frequency dependent) attenuation coefficient, $E_0(f)$ the power spectral density at a reference point and $E(f)$ is the power spectral density after attenuation by sea ice during a distance d. There is an implicit assumption that the attenuation coefficient does not change over the distance d.

We only use data where we have data from both buoys and where both buoys recorded a significant wave height of at least 0.1 m. During the spring deployment, SWIFT21 was deep in sea ice and did not record almost any wave activity for the first part of the deployment (Figure 4). We therefore only use data from 2019-10-31 to 2019-11-08, where SWIFT21 generally observed wave activity and SWIFT20 was in open water. The check factor was generally $\ll 1$ when $E(f) < 10^{-4}\,\text{m}^2/\text{Hz}$, which was true for most part of the spectrum in sea ice (Figure 4). We attribute this to wave attenuation below the instrument noise level, and therefore only focus on the frequency band $0.05 \leq f \leq 0.13\,\text{Hz}$ for this study. In total, this filtering resulted in 36 data point pairs in winter and 100 data point pairs in spring, for each of the seven analysed frequency bins.

For each pair of data points, the attenuation coefficient was defined as

$$\alpha(f) = \frac{\ln(E_{\mathrm{SWIFT20}}(f)) - \ln(E_{\mathrm{SWIFT21}}(f))}{d} \quad (6)$$

where the power spectral density measurement by SWIFT20 was used as the reference value. In winter, both buoys were in the ice, and we defined d as the effective separation between the both buoys along the incident wave direction. For each time stamp, we defined the incident wave direction as the average of the energy weighted wave direction between the two buoys. In spring, SWIFT20 was in open water, and d was then defined as the distance from SWIFT21 to the ice edge in the energy weighted wave direction as measured in sea ice by SWIFT21.

We did not account for the time it would take for waves to travel the effective separation between SWIFT20 and SWIFT21. For the analysed frequency band, this corresponds to a time delay of 2-5 hours per 100 km based on the dispersion relation for linear waves in deep water. In winter, the buoys were so close that this time lag is shorter than the time resolution. Even though the time lag in spring is large, the temporal variation in spectral energy density is small compared to the difference between buoys. The effect of the time delay on the estimated attenuation coefficient is therefore expected to be small compared to other uncertainties.

3 Result and discussion

The significant wave height measured by the buoys were around 0.5-1 m during the winter deployment. In spring, SWIFT20 generally measured significant wave heights around 0.2 m while in ice, with two notable events where the significant wave height increased to almost 1 m (Figure 4). While in open water, SWIFT20 measured significant wave heights between 1.5 – 3 m. SWIFT21 was arguably not in the MIZ during the first 9 days as almost no wave activity was recorded (Figure 4).

The maximum observed wave height was 2.7 m in open water (SWIFT20, November 17) and 1.7 m in ice (SWIFT20, October 23). No significant wave activity was observed more than 200 km from the ice edge in wave direction (150 km from ice edge closest direction) (Figure 5b). Wave activity was observed in 100 % sea ice concentration (Figure 4), illustrating that waves can reach beyond the sea ice concentration-based definition of the MIZ.

The measured wave spectra and significant wave height illustrates some of the key effects sea ice has on surface waves. In the ice, the significant wave height is typically much lower (Figure 1c-d), and the high frequency content diminishes (Figure 4c,f). One notable event is the transition from sea ice to open water by SWIFT20 around 31 October. This event is seen as a steep increase in significant wave height as well as an increase in higher frequency content of several orders of magnitude, and is confirmed by SWIFT on-board imagery (Figure 4a-c). It coincides fairly well with the co-located sea ice concentration. Between 2-4 November, when SWIFT20 is in open water, there are three instances where the high frequency content drops. The first one occurred during the dark hours, thus lacking on-board imagery, but for the other two on-board imagery confirms that this is due to sea ice.

3.1 Spectral wave attenuation

Box-and-whisker plots of the observed attenuation coefficients is shown in Figure 5, together with non-linear least square fits to the power law

$$\alpha(f) = af^b \quad (7)$$

The fitted parameters are presented in Table 2. A clear trend with increasing attenuation for increasing frequencies is seen. No roll over effect is observed, which indicates

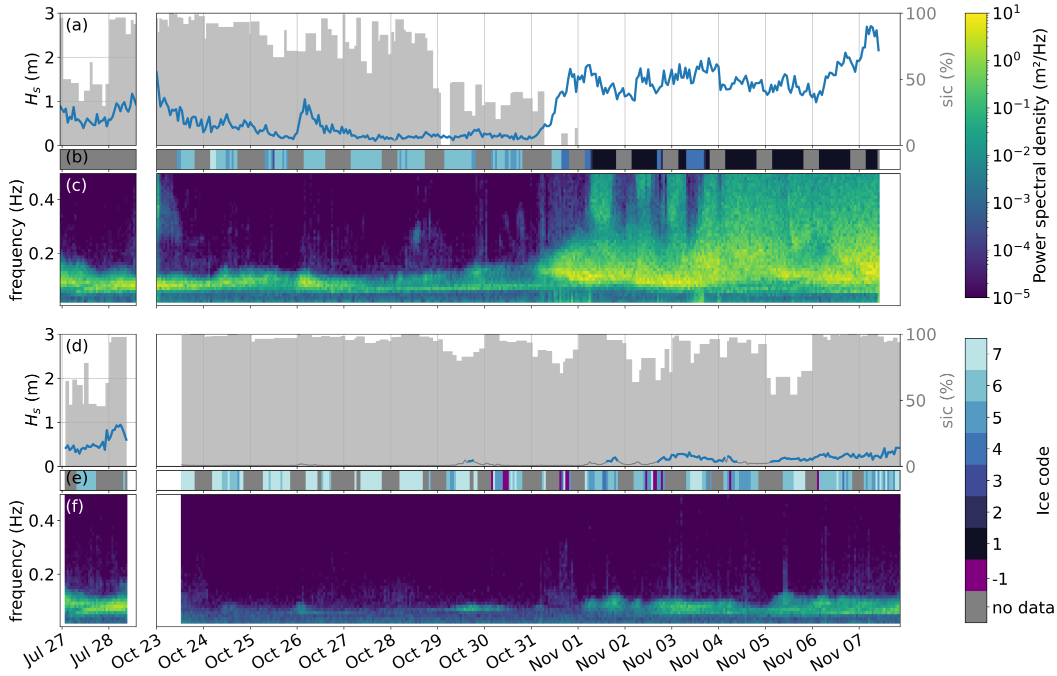

Figure 4. Overview of the data collected by SWIFT20 (top) and SWIFT21 (bottom) in winter (left panels) and spring (right panels). (a,d) Significant wave height (blue line) and wave spectra measured by SWIFT, together with co-located sea ice concentration (shaded grey) from AMSR-E. Significant wave height of less than 0.1 m is shown in grey. (b,e) Local ice condition based on SWIFT on-board imagery. (c,f) Spectral power density.

Table 2. Parameter estimates for the power law $\alpha = af^b$, using non-linear least squares.

deployment	a	b	constraint
spring	0.065	3.3	none
winter	8.4	4.9	none
winter	1.3	4.0	$2 \leq b \leq 4$

that the data filtering process described in section 2.6 was successful in avoiding spurious negative biases from instrument noise.

Attenuation rates for both spring and winter are in the order of magnitudes 10^{-5}–$10^{-4}\,\mathrm{m}^{-1}$. The attenuation coefficient is roughly 5 times larger in winter than spring, but both the winter and spring observations are consistent with previous observations in the Antarctic MIZ (Figure 6). SWIFT on-board imagery and ship observations show that the buoys were clearly in the break-up region (or open water) during the part of the deployments used for deriving wave attenuation.

No significant attenuation is seen for the lowest frequency bins in winter (Figure 5). Since the distance between buoys were around 10 km, an attenuation coefficient α of $10^{-5}\mathrm{m}^{-1}$ would result in a difference of power density spectrum of only 10%, which is probably too low to measure given the circumstances.

The frequency dependence of the attenuation rate is consistent with power law for both data sets (Figure 5). In spring, the fitted power coefficient $b = 3.3$ is consistent with the constraint $2 \leq b \leq 4$ suggested in (Meylan et al., 2018). In winter, the curve fit gave $b = 4.9$, higher than the predictions by Meylan et al, but adding a constraint $2 \leq b \leq 4$ results in a very similar fit (Figure 5a). Since no measurable attenuation is seen for the lower frequency bins in winter, fitting a two parameter model to this data set is prone to overfitting. It is clear that b lies in the higher region of those predicted by Meylan et al, but too much weight should not be put on the exact value.

The ice condition during the winter deployment was similar for the whole data set in the area around the buoys. Thanks to extensive ice observations from the ship, (Skatulla et al., 2022), (de Vos et al., 2019), the ice condition is well described.

In contrast to the winter deployment, the attenuation should be seen as an integrated effect over a wide range of ice conditions (covering all from the transition from open water to more than 100 km into the MIZ). Even so, it is worth noting that the spring deployment is much deeper into the MIZ and in higher sea ice concentration, while experiencing a much lower attenuation rate.

3.2 Change in wave direction

Figure 7a shows the energy weighted wave direction of the swell band $0.05 \leq f \leq 0.13$ Hz for the spring deployment as a function of distance to the ice edge. The cluster of points 2019-10-24 to 2019-10-27 is collected by SWIFT20 and associated with a rapid northward movement of the ice edge (Figure 2c) and two wave events (Figure 4a). We therefore believe that this cluster belongs to another wave field, not representative for the rest of the deployment. Apart from this cluster, a clear trend is seen, where the wave direction tends to be more towards the south, and thus more perpendicular to the ice edge, with increasing distance travelled in sea ice.

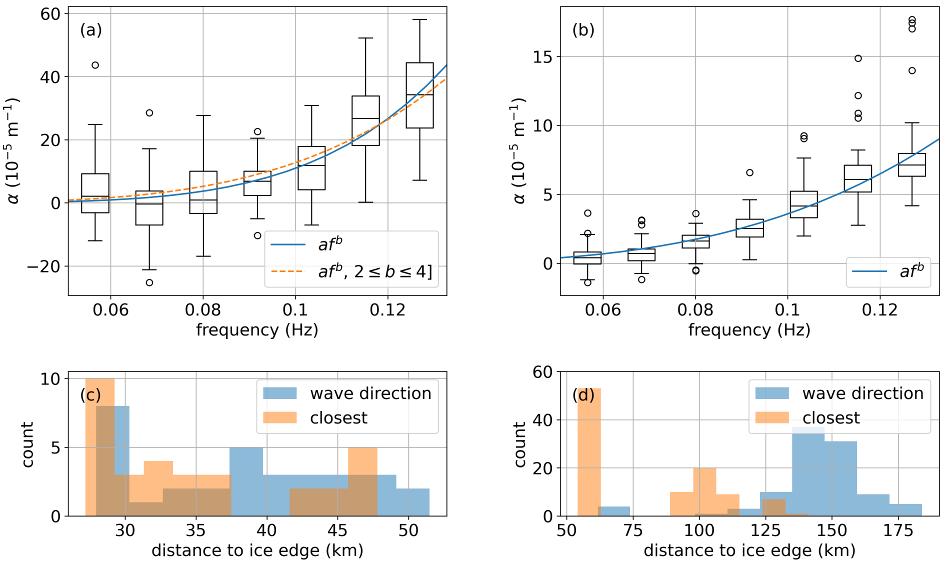

Figure 5. (top) Box-and-whisker plots of the attenuation rates as a function of wave frequency, together with power law-fits. The fitted parameters are presented in Table 2. a) Data from the winter deployment, where the distance in wave direction between the buoys was around 16 km. Each frequency bin has 36 data points. b) Data from the spring deployment, where one buoy was in open water and the other in sea ice. Each frequency bin has 100 data points. (bottom) Histogram of the distance to the ice edge for the two data sets in (c) winter (mean of the two buoys) and (d) spring.

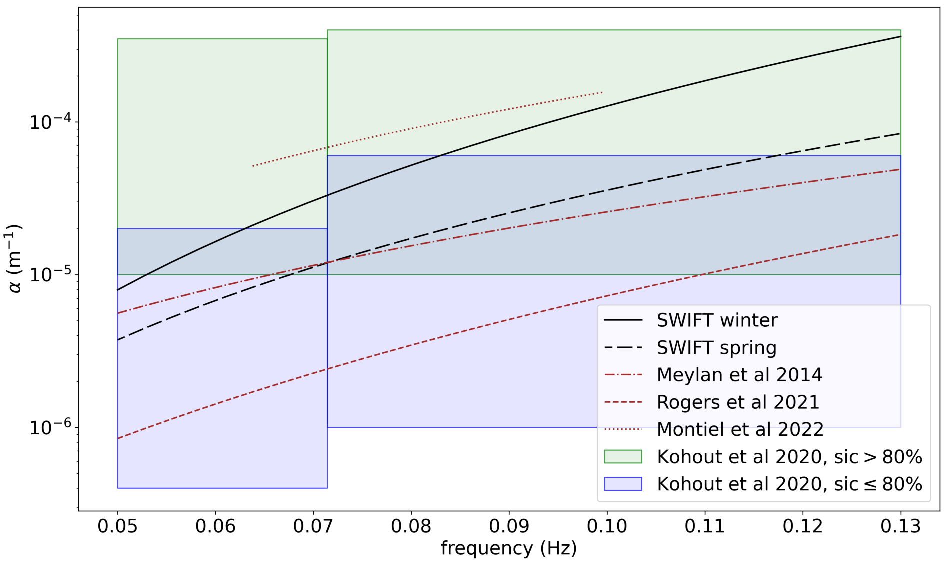

Figure 6. Comparison with other observations of spectral wave attenuation in the Antarctic MIZ: Attenuation based on the SIPEX-II data set in September 2012 Meylan et al. (2014) and various derivations from the large PIPERS data set presented by Kohout et al. (2020). W. E. Rogers et al. (2021) used the eastern subset of this data set, collected in June 2017, while the western subset, collected in April-May 2017, was used by Montiel et al. (2022).

In order to further study this effect, we binned the data into 50 km-groups based on the closest distance to the ice edge. Data points before 2019-10-28 were excluded from analysis based on the reasoning above. The change in wave direction coincides with an increase in sea ice concentration and a decrease in directional spread (Figure 7b-d).

A strong correlation between distance to ice edge and wave direction is observed. Since the two buoys drifted towards the ice edge during the deployment, distance to the ice edge and time is highly correlated in this data set. Therefore, the finding should account for this. Still, the same trend is seen where we have simultaneous measurements for both buoys (Figure 7a). Since in-situ measurements of wave direction in the Antarctic MIZ is rare, (the most extensive data sets are from WIIOS buoys, which does not provide direction measurements), we find these results valuable enough to report. A similar observation has been made from Sentinel-1 SAR data in the Barents Sea (Monteban et al., 2019). We see two plausible mechanisms that could cause wave direction to shift towards normal with increasing distance from the ice edge: an actual change in wave direction due to refraction, or an apparent change in wave direction due to wave attenuation (spatial filtering).

If the observed change in wave direction is caused by refraction, it would mean that the waves slow down (group speed decreases) as they propagate through the sea ice. It is important to point out that refraction happens due to changes in the dispersion relation. This is distinct from wave attenuation, which does not require a change in the medium (on the contrary, it is typically assumed a constant attenuation in order to be able to quantify it from observations). In order for refraction to explain the continuous change in dominant wave direction observed in the data, there must therefore be a continuous change in the dispersion relation, where waves progressively slow down as they travel further into the ice. Figure 7c shows a change in co-located sea ice concentration that matches the observed change in wave direction. Note that at these scales, the sea ice concentration may be seen as a proxy for the overall ice condition. We know from the SWIFT onboard imagery that the sea ice quality changes drastically between measurements close to the ice edge and far into the sea ice.

Actual surface waves will always have a spread in direction, i.e. the waves do not have exactly the same direction. This means that even if the open water wave field was entirely homogeneous, the waves reaching a certain point in the sea ice would come from different directions, and thus have travelled different distances in the sea ice. This means that the waves with a more oblique incidence angle would have travelled farther, and therefore would be more attenuated, shifting the dominant direction towards normal while decreasing the directional spread. We do observe some decrease in directional spread with increasing distance from the ice edge (Figure 7c), but further analysis is required to determine if this decrease is enough to explain the change in direction.

4 Summary

Two wave buoys were deployed in the Atlantic Antarctic MIZ during the SCALE cruises in austral winter and spring in 2019 to observe wave-sea ice interactions. No wave activity was observed more than 200 km into the MIZ, while the open water wave field had a significant wave height around 2-3 m in spring.

From this data set, we have derived spectral wave attenuation coefficients for wave frequencies between 0.05 and 0.13 Hz. The attenuation coefficients were around $4{\cdot}10^{-6}$ to $7{\cdot}10^{-5}\,\mathrm{m}^{-1}$ in spring, and approximately five-fold larger in winter. This is in agreement with in-situ studies of the Pacific Antarctic MIZ. The frequency dependent is consistent with a power law dependency, with a power coefficient of around 4 in winter and 3.3 in spring.

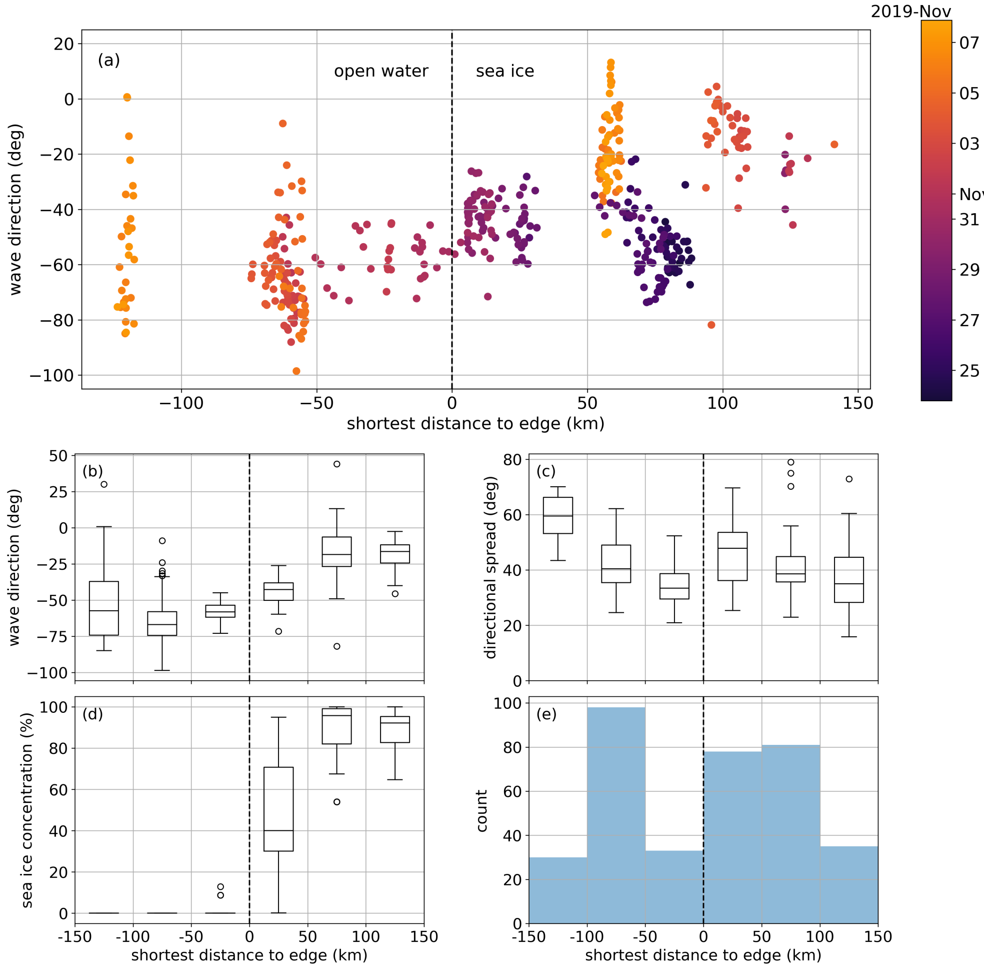

Figure 7. Energy weighted wave direction of the swell band $0.05 \leq f \leq 0.13$ as a function of distance to the ice edge, measured by SWIFT buoys during the spring deployment. (a) Scatter plot of all measurements, coloured by time. (b-d) Box-and-whisker plots of (b) wave direction, (c) directional spread and (d) co-located sea ice concentration, collected after 2019-10-27, binned by distance to the ice edge. The number of data points per bin is shown in (e).

A relationship between wave direction and distance to ice edge was observed in the data, where the wave direction tends to be more perpendicular to the ice edge deeper in sea ice. This could be a sign of refraction, where the propagation velocity changes with sea ice condition.

Acknowledgments

This work was supported by the following grants of S. Swart: Wallenberg Academy Fellowship (WAF 2015.0186), Swedish Research Council (VR 2019-04400), STINT-NRF Mobility Grant (STNT180910357293). S. Swart has received funding from the European Union's Horizon 2020 research and innovation program under Grant agreement no. 821001 (SO-CHIC). L.C Biddle's time was supported by the VR grant 2020-04281. Alex de Klerk and Joe Talbert built and prepared the SWIFT buoys. The authors thank Sea Technology Services (STS), SANAP, the Captain, and crew of the S.A. Agulhas II for their fieldwork/technical assistance. The authors also thank Isabelle Giddy, Hanna Rosenthal, Johan M. Edholm, Kevin Thielen and all other participants of the SCALE cruises who helped with deployment, spotting and recovery of the SWIFT buoys.

Data Availability Statement

The sea-ice data is made available via `https://seaice.uni-bremen.de/databrowser/`. Sentinel-1 SAR imagery is available via `https://dataspace.copernicus.eu/browser/`. The code used for this analysis is available at `https://github.com/stinawahlgren/roammiz-wave-seaice-interactions` and SWIFT buoy data is available at `https://doi.org/10.5281/zenodo.7845764`. SWIFT buoy data has been processed using `https://github.com/SASlabgroup/SWIFT-codes`.

References

Ardhuin, F., Otero, M., Merrifield, S., Grouazel, A., & Terrill, E. (2020). Ice Breakup Controls Dissipation of Wind Waves Across Southern Ocean Sea Ice. *Geophysical Research Letters*, *47*(13), e2020GL087699. Retrieved from `https://onlinelibrary.wiley.com/doi/abs/10.1029/2020GL087699` doi: 10.1029/2020GL087699

Cooper, V. T., Roach, L. A., Thomson, J., Brenner, S. D., Smith, M. M., Meylan, M. H., & Bitz, C. M. (2022, September). Wind waves in sea ice of the western Arctic and a global coupled wave-ice model. *Philosophical Transactions of the Royal Society A: Mathematical, Physical and Engineering Sciences*, *380*(2235), 20210258. Retrieved from `https://royalsocietypublishing.org/doi/10.1098/rsta.2021.0258` doi: 10.1098/rsta.2021.0258

de Vos, M., Ramjukadh, C.-L., Liesker, C. G., de Villiers, M., & Lyttle, C. T. (2019, September). *Southern Ocean Marginal Ice Zone Photographs from a 2019 Winter Research Cruise (SA Agulhas II).* PANGAEA. Retrieved from `https://doi.pangaea.de/10.1594/PANGAEA.905497` doi: 10.1594/PANGAEA.905497

Hošeková, L., Malila, M. P., Rogers, W. E., Roach, L. A., Eidam, E., Rainville, L., … Thomson, J. (2020). Attenuation of Ocean Surface Waves in Pancake and Frazil Sea Ice Along the Coast of the Chukchi Sea. *Journal of Geophysical Research: Oceans*, *125*(12), e2020JC016746. Retrieved from `https://onlinelibrary.wiley.com/doi/abs/10.1029/2020JC016746` doi: 10.1029/2020JC016746

Kohout, A. L., Smith, M., Roach, L. A., Williams, G., Montiel, F., & Williams, M. J. M. (2020, September). Observations of exponential wave attenuation in Antarctic sea ice during the PIPERS campaign. *Annals of Glaciology*, *61*(82), 196–209. Retrieved from `https://www.cambridge.org/core/journals/`

annals-of-glaciology/article/observations-of-exponential-wave-attenuation-in-antarctic-sea-ice-during-the-pipers-campaign/A21809218DA23F5DE46CC0D823922A55 doi: 10.1017/aog.2020.36

Kousal, J., Voermans, J. J., Liu, Q., Heil, P., & Babanin, A. V. (2022). A Two-Part Model for Wave-Sea Ice Interaction: Attenuation and Break-Up. *Journal of Geophysical Research: Oceans*, *127*(5), e2022JC018571. Retrieved from https://onlinelibrary.wiley.com/doi/abs/10.1029/2022JC018571 doi: 10.1029/2022JC018571

Langhorne, P. J., Squire, V. A., Fox, C., & Haskell, T. G. (1998/ed). Break-up of sea ice by ocean waves. *Annals of Glaciology*, *27*, 438–442. Retrieved from https://www.cambridge.org/core/journals/annals-of-glaciology/article/breakup-of-sea-ice-by-ocean-waves/DCDE1C3D4F33A59B8EE12DC940DB0F61 doi: 10.3189/S0260305500017869

Li, J., Kohout, A. L., Doble, M. J., Wadhams, P., Guan, C., & Shen, H. H. (2017). Rollover of Apparent Wave Attenuation in Ice Covered Seas. *Journal of Geophysical Research: Oceans*, *122*(11), 8557–8566. Retrieved from https://onlinelibrary.wiley.com/doi/abs/10.1002/2017JC012978 doi: 10.1002/2017JC012978

Massom, R. A., Scambos, T. A., Bennetts, L. G., Reid, P., Squire, V. A., & Stammerjohn, S. E. (2018, June). Antarctic ice shelf disintegration triggered by sea ice loss and ocean swell. *Nature*, *558*(7710), 383–389. Retrieved from https://www.nature.com/articles/s41586-018-0212-1 doi: 10.1038/s41586-018-0212-1

Melsheimer, C. (2019). *ASI Version 5 Sea Ice Concentration User Guide.*

Melsheimer, C., & Spreen, G. (2019, February). *AMSR2 ASI sea ice concentration data, Antarctic, version 5.4 (NetCDF) (July 2012 - December 2019).* PANGAEA. Retrieved from https://doi.pangaea.de/10.1594/PANGAEA.898400 doi: 10.1594/PANGAEA.898400

Meylan, M. H., Bennetts, L. G., & Kohout, A. L. (2014). In situ measurements and analysis of ocean waves in the Antarctic marginal ice zone. *Geophysical Research Letters*, *41*(14), 5046–5051. Retrieved from https://onlinelibrary.wiley.com/doi/abs/10.1002/2014GL060809 doi: 10.1002/2014GL060809

Meylan, M. H., Bennetts, L. G., Mosig, J. E. M., Rogers, W. E., Doble, M. J., & Peter, M. A. (2018). Dispersion Relations, Power Laws, and Energy Loss for Waves in the Marginal Ice Zone. *Journal of Geophysical Research: Oceans*, *123*(5), 3322–3335. Retrieved from https://onlinelibrary.wiley.com/doi/abs/10.1002/2018JC013776 doi: 10.1002/2018JC013776

Monteban, D., Lubbad, R., & Johnsen, H. (2019). Sentinel-1 sar observations of peak wavelength and dominant wave direction in the marginal ice zone of the barents sea. *Proceedings - International Conference on Port and Ocean Engineering under Arctic Conditions*. Retrieved from https://ntnuopen.ntnu.no/ntnu-xmlui/handle/11250/2639926

Montiel, F., Kohout, A. L., & Roach, L. A. (2022, May). Physical Drivers of Ocean Wave Attenuation in the Marginal Ice Zone. *Journal of Physical Oceanography*, *52*(5), 889–906. Retrieved from https://journals.ametsoc.org/view/journals/phoc/52/5/JPO-D-21-0240.1.xml doi: 10.1175/JPO-D-21-0240.1

Montiel, F., Squire, V. A., Doble, M., Thomson, J., & Wadhams, P. (2018). Attenuation and Directional Spreading of Ocean Waves During a Storm Event in the Autumn Beaufort Sea Marginal Ice Zone. *Journal of Geophysical Research: Oceans*, *123*(8), 5912–5932. Retrieved from https://onlinelibrary.wiley.com/doi/abs/10.1029/2018JC013763 doi: 10.1029/2018JC013763

Rogers, W., Posey, P., Li, L., & Allard, R. (2018, April). Forecasting and Hindcasting Waves In and Near the Marginal Ice Zone: Wave Modeling and the ONR Sea State Field Experiment.. Retrieved from https://www.semanticscholar

.org/paper/Forecasting-and-Hindcasting-Waves-In-and-Near-the-Rogers-Posey/5583f6d20c399b17bbebd4efc347c0bb0b69a01a

Rogers, W. E., Meylan, M. H., & Kohout, A. L. (2021, February). Estimates of spectral wave attenuation in Antarctic sea ice, using model/data inversion. *Cold Regions Science and Technology*, *182*, 103198. Retrieved from https://www.sciencedirect.com/science/article/pii/S0165232X20304456 doi: 10.1016/j.coldregions.2020.103198

Shen, H. H., & Ackley, S. F. (1991/ed). A one-dimensional model for wave-induced ice-floe collisions. *Annals of Glaciology*, *15*, 87–95. Retrieved from https://www.cambridge.org/core/journals/annals-of-glaciology/article/onedimensional-model-for-waveinduced-icefloe-collisions/32F3295E93860E65517AE0310F8033C7 doi: 10.3189/1991AoG15-1-87-95

Skatulla, S., Audh, R. R., Cook, A., Hepworth, E., Johnson, S., Lupascu, D. C., ... Vichi, M. (2022, July). Physical and mechanical properties of winter first-year ice in the Antarctic marginal ice zone along the Good Hope Line. *The Cryosphere*, *16*(7), 2899–2925. Retrieved from https://tc.copernicus.org/articles/16/2899/2022/ doi: 10.5194/tc-16-2899-2022

Squire, V. A. (2018, August). A fresh look at how ocean waves and sea ice interact. *Philosophical Transactions of the Royal Society A: Mathematical, Physical and Engineering Sciences*, *376*(2129), 20170342. Retrieved from https://royalsocietypublishing.org/doi/full/10.1098/rsta.2017.0342 doi: 10.1098/rsta.2017.0342

Thomson, J. (2012, December). Wave Breaking Dissipation Observed with "SWIFT" Drifters. *Journal of Atmospheric and Oceanic Technology*, *29*(12), 1866–1882. Retrieved from https://journals.ametsoc.org/view/journals/atot/29/12/jtech-d-12-00018_1.xml doi: 10.1175/JTECH-D-12-00018.1

Thomson, J. (2022, September). Wave propagation in the marginal ice zone: Connections and feedback mechanisms within the air–ice–ocean system. *Philosophical Transactions of the Royal Society A: Mathematical, Physical and Engineering Sciences*, *380*(2235), 20210251. Retrieved from https://royalsocietypublishing.org/doi/10.1098/rsta.2021.0251 doi: 10.1098/rsta.2021.0251

Thomson, J., Girton, J. B., Jha, R., & Trapani, A. (2018, February). Measurements of Directional Wave Spectra and Wind Stress from a Wave Glider Autonomous Surface Vehicle. *Journal of Atmospheric and Oceanic Technology*, *35*(2), 347–363. Retrieved from https://journals.ametsoc.org/view/journals/atot/35/2/jtech-d-17-0091.1.xml doi: 10.1175/JTECH-D-17-0091.1

Thomson, J., Hošeková, L., Meylan, M. H., Kohout, A. L., & Kumar, N. (2021). Spurious Rollover of Wave Attenuation Rates in Sea Ice Caused by Noise in Field Measurements. *Journal of Geophysical Research: Oceans*, *126*(3), e2020JC016606. Retrieved from https://onlinelibrary.wiley.com/doi/abs/10.1029/2020JC016606 doi: 10.1029/2020JC016606

Thomson, J., Talbert, J., de Klerk, A., Brown, A., Schwendeman, M., Goldsmith, J., ... Meinig, C. (2015, June). Biofouling Effects on the Response of a Wave Measurement Buoy in Deep Water. *Journal of Atmospheric and Oceanic Technology*, *32*(6), 1281–1286. Retrieved from https://journals.ametsoc.org/view/journals/atot/32/6/jtech-d-15-0029_1.xml doi: 10.1175/JTECH-D-15-0029.1

Toffoli, A., Bennetts, L. G., Meylan, M. H., Cavaliere, C., Alberello, A., Elsnab, J., & Monty, J. P. (2015). Sea ice floes dissipate the energy of steep ocean waves. *Geophysical Research Letters*, *42*(20), 8547–8554. Retrieved from https://onlinelibrary.wiley.com/doi/abs/10.1002/2015GL065937 doi: 10.1002/2015GL065937

Vichi, M., Eayrs, C., Alberello, A., Bekker, A., Bennetts, L., Holland, D., ... Toffoli, A. (2019). Effects of an Explosive Polar Cyclone Crossing the Antarctic

Marginal Ice Zone. *Geophysical Research Letters*, *46*(11), 5948–5958. Retrieved from https://onlinelibrary.wiley.com/doi/abs/10.1029/2019GL082457 doi: 10.1029/2019GL082457

Voermans, J. J., Babanin, A. V., Thomson, J., Smith, M. M., & Shen, H. H. (2019). Wave Attenuation by Sea Ice Turbulence. *Geophysical Research Letters*, *46*(12), 6796–6803. Retrieved from https://onlinelibrary.wiley.com/doi/abs/10.1029/2019GL082945 doi: 10.1029/2019GL082945

Wadhams, P., Squire, V. A., Goodman, D. J., Cowan, A. M., & Moore, S. C. (1988). The attenuation rates of ocean waves in the marginal ice zone. *Journal of Geophysical Research: Oceans*, *93*(C6), 6799–6818. Retrieved from https://onlinelibrary.wiley.com/doi/abs/10.1029/JC093iC06p06799 doi: 10.1029/JC093iC06p06799